Hindawi
International Journal of Aerospace Engineering
Volume 2020, Article ID 2180927, 12 pages
https://doi.org/10.1155/2020/2180927

Research Article

Numerical and Experimental Failure Analysis of Carbon Fiber-Reinforced Polymer-Based Pyrotechnic Separation Device

Mingfa Ren,[1] Fei Weng,[1] Jing Sun,[2] Zhifeng Zhang,[2] Zhiguo Ma,[3] and Tong Li[1]

[1]*Department of Engineering Mechanics, Dalian University of Technology, Dalian 116024, China*
[2]*Beijing Institute of Astronautical Systems Engineering, Beijing 100076, China*
[3]*Nanjing Research Institute of Simulation Technology, Nanjing 210000, China*

Correspondence should be addressed to Tong Li; tong@dlut.edu.cn

Received 13 September 2019; Revised 21 November 2019; Accepted 7 December 2019; Published 7 January 2020

Academic Editor: Nicolas Avdelidis

Current pyrotechnic separation devices are mainly made of metal materials, limiting the capacity of lightweight design in advanced launching vehicles. With the outstanding mechanical properties, such as high mass-specific strength and modulus, carbon fiber-reinforced polymers (CFRPs) have the potential to replace metal materials in pyrotechnic seperaton devices. However, to improve the seperation reliability of these pyrotechnic separation devices, there still needs further understanding on the the failure mode of CFRP composites under linear shaped charge (LSC). In this paper, cutting tests were carried out on CFRPs for the failure analysis of CFRPs under LSC, and nonlinear finite element analysis (FEA) was performed to characterize the evolution of LSC cutting in CFRPs. According to experimental simulation and numerical simulation, it can be found that the three main failure modes in CERPs while subjected to LSC jet are shear failure, delamination failure, and tensile failure. In the early cutting stage, the initial time of damage of the fiber and the matrix near the shaped charge shows less difference and the laminate is directly separated by the energy of high-speed jet. When the jet velocity decreases, the jet morphology collapses and matrix damages precede into the fiber, which would cause tensile failure mode of CFRPs. Meanwhile, the delamination in low jet speed stages is larger than that in the high jet speed stages. These studies on the failure modes of CFRPs under LSC provide important basis for the future design of CFRP-based pyrotechnic separation devices, which is important to the lightweight design of launching vehicles.

1. Introduction

Aerospace separation device plays important roles in the launching process of space vehicles. Pyrotechnic separation device is a commonly used which is mainly composed of a separation shell, driving force provider, protective structure, and fixed structure, as illustrated in Figure 1. To date, the separation shell mostly employs metal materials. The new generation of separation devices targets to replace the metal materials with CFRP composites to achieve the lightweight design, which would improve the carrying capacity of the rockets. Shaped charge is one of main driving forces for explosive separation devices. LSC is a pyrotechnic cutting device based on the mohaupt effect. The basic principle is as follows: when the detonator is fired, the detonation wave of explosion acts on the metal liner and makes it press along with the axis with high velocity. The metal liner deforms and impacts each other. At high impulse force, the liner's melting and gasifying creates high-energy metal jets which is forced to gather along the axis, then penetrate or cut the target material and achieve separation operation [1]. Since the material's property is isotropic and homogeneous, researches on the cutting of metal materials subjected to shaped charge jet are relatively mature. The cutting tests on steel plate was carried out against the shaped charge jet [2, 3], and it was found that the cutting length of the shaped charge shall be longer than that of the steel plate. Lyu et al. [4] experimentally evaluated the cutting of Ti alloy target which applied in the engine fan blade. After cutting, the upper section of the Ti alloy near the shaped charge is smooth and has a metallic shine due to jet adhesion for the stages of crater formation and the first quasi-steady penetration. The lower section away from the

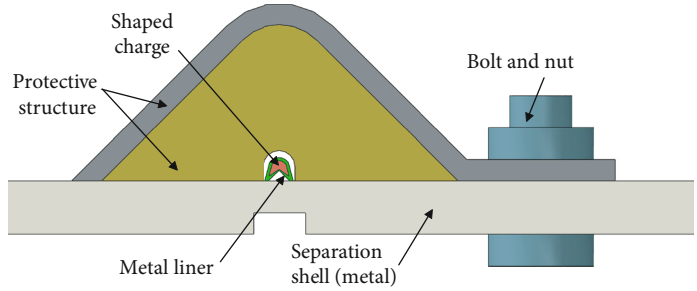

Figure 1: General aerospace separation device.

shaped charge appears fish scale which suffers from both penetration and spallation. The cutting test on Al plate with protective cover was also carried out, and the results show that there are mainly two sections of fractures, which the were similar to those in Lyu et al.'s research [5].

As the typical anisotropic material, CFRPs result in different failure modes from that of metal materials. The insightful understanding of the CFRP's failure under LSC jet is significant to the optimization of CFRP-based separation devices. Firstly, the cutting of CFRPs has an effect on jet morphology and penetration damage area. Compared with steel-only structures, the sandwich plate made of two steel shells and a compact polyurethane has a smaller damage zone due to the assistance of the polymer layer [6]. For woven fabric rubber composites, Jia et al. [7] pointed out that when subjected to a large-area ablation, the fiber yarns were significantly pulled out from the woven fabric by the jet impact. The disordered distribution of yarns causes large disturbance effect to the jet, which has better protection capability. When the jet penetrates the composite target, the woven composites appear as a large opening displacement, a scale of debonding and delamination also appear, and the dominating failure mode is shear brittle failure [7]. However, these abovementioned researches on the failure of composite materials against shaped charge jet are not strictly designed for the CFRPs in aerospace structures. It is urgent to have more specific study on the failure of CFRPs under LSC, which could be applied to the design on lightweight launching vehicles.

At present, the research on the high-speed impact failure of CFRPs mainly focuses on projectile impact. High-velocity tests on composites using flat, hemispherical, and conical projectiles have shown shear failure in plies nearest the impact surface to be the initial failure mode. Subsequent damage modes depend on the materials, fiber architecture, and ply layups but often include delamination and fiber tensile failure in the interior or near the back surface plies [8]. Kapoor et al. [9] explored the possible failure modes based on experimental investigations on kevlar fiber-reinforced polypropylene woven composites. The main failure modes include delamination, fiber failure, and shear fracture under high loading strain rate. For CFRPs, Lee and Sun [10] experimentally evaluated the dynamic penetration of laminates and defined the penetration process in three diffierent stages: plugging, predelamination (fiber crushing), and postdelamination. In addition, the ballistic tests were carried out on the impact velocity ranging between 610 and 1830 m/s. The three stages of the damage process include (i) punching, (ii) fiber breaking, and (iii) delamination, which were believed to provide the main energy absorption capacity during the penetration process and the cause of the deceleration of the projectile [11]. However, compared to the projectile, the impact caused by the speed of the shaped charge jet is much greater. Meanwhile, the jet form is a plastic flow, which is significantly different from the projectile impact. Under such a loading condition, there needs more investigation on the failure modes of composites. In addition, the above projectile impact studies can record the failure process of laminates by high-speed camera, but the cutting test of laminates can only show the final fracture morphology under high-speed jet due to the short action time and the presence of smoke. In terms of simulation, finite element method (FEM) [12] is suitable for the structural analysis, and it is effective to simulate complex impact processes with a low computational expense. Arbitrary Lagrange-Euler (ALE) methods [13] have been applied to solve the deformation problem under the action of shaped charge jet. The simulation can characterize the evolution of failure in the laminate. However, for the large deformation and nonlinear simulation calculation on the jet cutting of composites, the simulation needs test results to support the rationality of the model.

In this paper, experiments and simulation are combined to explore the failure modes of CFRPs under the action of shaped charge jet. Firstly, the test of CFRP separation device subjected to shaped charge jet is carried out for the study on macroscopic and microscopic fracture morphology. Compared to the separation structure [5], the protective structure in the test is equipped with buffer material. Then, the modeling investigation of composites separation device is conducted to characterize the cutting process of composites. The simulation model takes into account the laminate delamination caused by the tiebreak contact. The cutting damage process of laminates is summarized from the aspect of the cutting process of the laminate, jet velocity, jet shape, and in-plane failure of the laminate. At last, the failure modes and the evolution process of CFRP laminates subjected to shaped charge jet are revealed by both experiments and simulation.

2. Tests and Simulation Models

2.1. Cutting Tests for Composites Separation Device. The cutting test of CFRP separation device is illustrated in Figure 2.

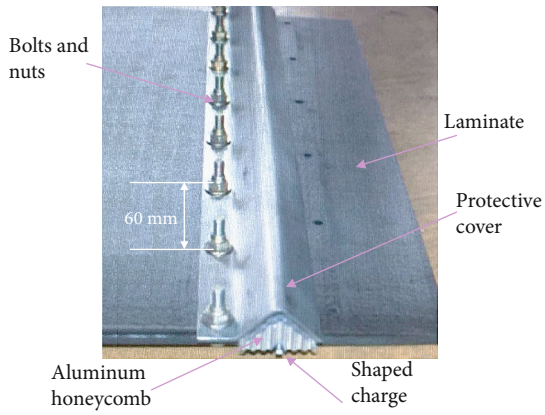

Figure 2: Cutting test of the composites separation device.

The laminate is made of bismaleimide resin-based CFRPs, formed into a stack in the specified fiber direction with heating and curing process. The lay-up is $[[45/-45/0/45/0/90/-45]_s]_2[0/30/\text{-}30/60/\text{-}60/0]$ according to the loading requirements and aerospace environment. The thickness of the laminate is 5.1 mm and the cutting thickness is 3 mm. The left and right boundaries of the laminate are clamped by two thick steel plates. The shaped charge is made of lead, and the V-shape structure is adopted for an ideal jet shape, jet velocity, and penetration depth. The shaped charge is attached to the surface of the laminate. In order to improve the cutting capacity, explosives with high detonation pressure (Hexogen) are selected and the density of explosive is 2.8-3.0 g/m. The test adopts single point initiation and linear cutting. The protective structure consists of a protective cover and a buffer structure. The protective cover is made of iron and the buffer structure is made of aluminum honeycomb materia.

2.2. Numerical Simulations

2.2.1. FEA Model. All simulations were performed on the platform of a commercial FEM package of LS-DYNA [14, 15]. The FEA model of composites separation device is shown in Figure 3. The model includes a laminate, air, aluminum honeycomb, protective cover, bolts, nuts, and shaped charge made up of explosives, outer case, and shaped charge liner. The amount of explosives set in the numerical model is 3.1 g/m, which is consistent with the experiment. Lagrange arithmetic modeling was adopted to describe the deformation and damage of protective cover, bolts, nuts, aluminum honeycomb, and laminates. ALE method can handle large deformation problems under detonation shocks and was used to model the deformation of air, explosives, and shaped charge. The lay-up of the laminate is the same as that in the cutting test introduced in Section 2.1. The laminate has 34 layers and the thickness of each layer is 0.15 mm. Considering the linear cutting of the laminate, the cutting width of the FEA model is 15 mm. The laminate is completely constrained at both ends in all directions. The front and back of the shaped charge and air are imposed by the displacement constraints in the direction of cutting length, and the total amount of elements is 628,084.

In order to characterize the delamination of the laminate, the tiebreak contact between layers is defined. The tiebreak allows the separation of the surfaces and finally the failure of the tied surfaces will occur following failure criterion:

$$\left(\frac{|\sigma_n|}{\text{NFLS}}\right)^2 + \left(\frac{|\sigma_s|}{\text{SFLS}}\right)^2 \geq 1, \tag{1}$$

where NFLS is the tensile failure strength and SFLS is the shear failure strength of the adhesive. According to literature, the NFLS is set as 58.0 MPa and SFLS is set as 91.5 MPa [16].

2.2.2. Material Models in FEA. The simulation model mainly includes material constitutive model and state equation. Both the shaped charge liner and the outer case are made of lead. The material is simulated with Steinberg constitutive model and Gruneisen state equation [14, 15]. The air is simulated with Null constitutive model [14, 15] and the density is 0.001293 g/cm^3. The aluminum honeycomb material is modeled by a plastic kinematic constitutive model. The density, modulus, and yield stress are 2.78 g/cm^3, 73 GPa, and 75 MPa, respectively. The explosive adopts the model of the detonation of a high explosive and could be described as Jones-Wilkins-Lee (JWL) state equation [14, 15]. The pressure of JWL state equation is displayed in Eq. (2). Note that γ_0 is the mass density, D is the detonation velocity of the ratio of high explosive, and A, B, R_1, R_2, ω, and E are the parameters of JWL state equation. Its material parameters refer to Table 1.

$$p = A\left(1 - \frac{\omega}{R_1 V}\right)e^{-R_1 V} + B\left(1 - \frac{\omega}{R_2 V}\right)e^{-R_2 V} + \frac{\omega E}{V}. \tag{2}$$

The composite uses an orthogonal isotropic material model based on the continuous failure mechanism of Matzenmiller [17]. The failure criteria for composites follow these conditions.

(1) Tensile Fiber Mode.

$$f_1 = \left(\frac{\sigma_x}{X_t}\right)^2 - 1 \tag{3}$$

(2) Compressive Fiber Mode.

$$f_2 = \left(\frac{\sigma_x}{X_c}\right)^2 - 1 \tag{4}$$

(3) Tensile Matrix Mode.

$$f_3 = \left(\frac{\sigma_y}{Y_t}\right)^2 + \left(\frac{\tau}{S_c}\right)^2 - 1 \tag{5}$$

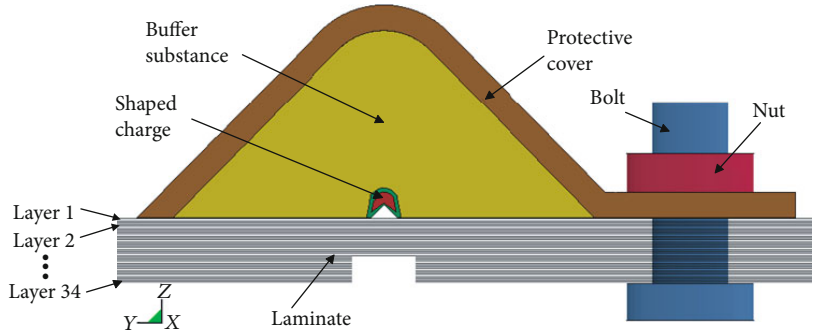

Figure 3: FEA model of the composites separation device.

Table 1: Material parameters of the explosive.

γ_0 (g/cm^3)	D (m/s)	P_{cj} (GPa)	A (GPa)	B (GPa)	R_1	R_2	ω	E_0 (GPa)
1.82	9110	39.3	778.3	7.071	4.2	1.0	0.34	8.5

(4) Compressive Matrix Mode.

$$f_4 = \left(\frac{\sigma_y}{Y_c}\right)^2 + \left(\frac{\tau}{S_c}\right)^2 - 1 \quad (6)$$

For the stiffness degradation for composites, Matzenmiller et al. [17] developed a constitutive equation of orthotropic damage composite based on continuous damage mechanics; they also introduced internal state variables to characterize the damage of composite materials and represented different damage modes by different state variables. Material stiffness degradation was achieved by the conversion of effective stress and true stress as shown in Eq. (7). The $\widehat{\sigma}$, σ, and M, respectively, represent effective stresses, true stresses, and rank-four damage operator.

$$\widehat{\sigma} = M\sigma. \quad (7)$$

In Table 2, the properties of the composite used are illustrated. E_a, E_b, and G (G_{ab}, G_{bc}, and G_{ca}) represent longitudinal modulus, transverse modulus, and shear modulus, respectively. X_c, X_t, Y_c, Y_t, and S_c are longitudinal compressive strength, longitudinal tensile strength, transverse compressive strength, transverse tensile strength, and shear strength, respectively.

2.2.3. Model Validation. To ensure the method validity of CFRPs' cutting simulation and rationality of the cutting model, use the simple cutting test result to validate the simulation model. The entire structure consists of a shaped charge and a laminate illustrated in Figure 4(a) [16]. In this validation test, the amount of explosive is about 3.85 g/m. The rationality of the numerical simulation model was validated by the comparision between the velocities of the feature points on the modeling laminate with the cutting tests. A test method with Displacement Interferometer System for Any Reflector (DISAR) was carried out. The FEA model for validation is shown in Figure 4(b). The amount of explosives is 3.9 g/m, which is consistent with the validation experiment. The size, ply, and thickness of laminates are all the same with the cutting test for model verification.

According to the cutting test, the velocity recorded by DISAR method is positive. Therefore, the data obtained by simulation are processed in absolute value. Because the accuracy of the test may be affected by the warping of laminates and the adhesion degree of aluminum foil after cutting, this paper only compares the cutting velocity in 35 μs, and velocity curve is shown in Figure 5. The result curve can be divided into three stages: (i) jet formation process; (ii) the cutting stage of the feature point position; and (iii) the cutting completion stage of feature point position. From the curve, the velocity is zero in the process of jet formation (stage i). In the second stage, the laminate is cut and the velocity is severe due to the propagation of stress wave. After the position of feature points on laminate is seperated, the velocity of the laminate approaches zero in both the cutting test and simulation (stage iii). The maximum velocity obtained by the simulation model is 19.73 m/s, which is 12.9% higher than the results obtained by the test (17.48 m/s). The volatility of shock wave can cause errors in the dynamic cutting simulation, while the numerical model can reproduce the experimental outcomes in a reasonable range, which proves the rationality of the simulation model.

3. Results and Discussion

These following sections discuss both test results and simulation results about the performance of the composites separation device. The experimental results are analyzed from two aspects: macroscale and microscale. The modeling results are discussed from the aspect of cutting process of the laminate, jet velocity, jet shape, and in-plane failure of the laminate.

Table 2: Material properties of unidirectional composites.

ρ_0 (g/cm^3)	E_a (GPa)	E_b (GPa)	ν_{ab}	G_{ab} (GPa)	G_{bc} (GPa)	G_{ca} (GPa)	X_c (GPa)	X_t (GPa)	Y_c (MPa)	Y_t (MPa)	S_c (MPa)
1.80	148	10.3	0.02	6.02	3.93	6.02	1.55	1.93	252	58	91.5

The subscript "a" is longitudinal direction and subscripts "b" and "c" are the transverse direction.

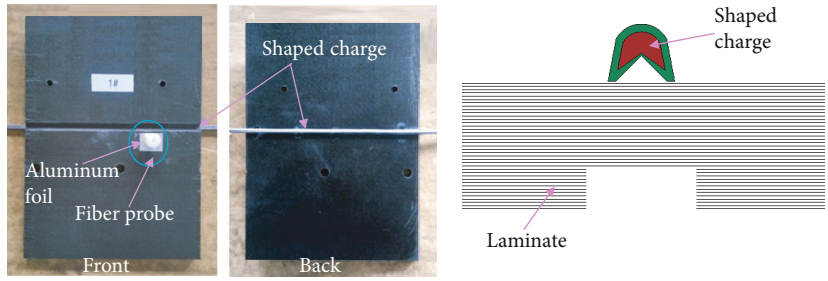

Figure 4: Cutting test and FEA model. (a) Cutting test for model verification [16]. (b) FEA model for verification.

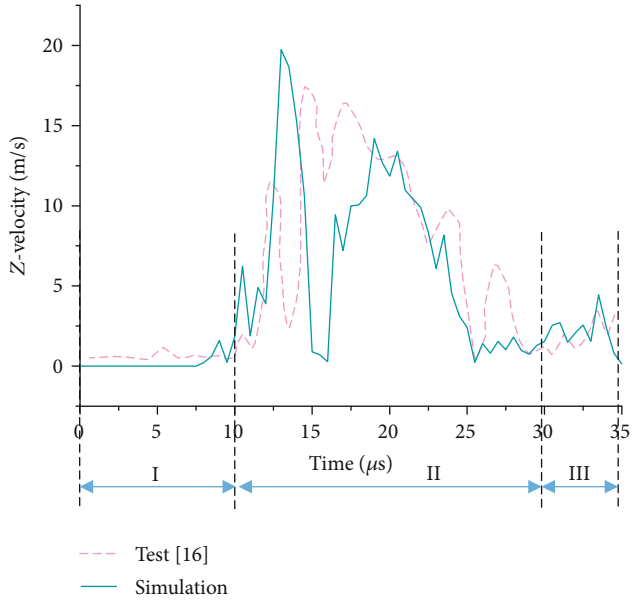

Figure 5: Velocity curves of the feature point of laminates.

3.1. Macroscopic Analysis of the Cutting Fracture. Figure 6(a) shows the separation performance of composites separation device subjected to LSC jet and the laminate was divided into two plates. Since the jet is in the thickness direction, the failure initiates from the top surface of the laminate. Figure 6(b) represents one-half of the laminate after cutting. It can be found that most of the laminate materials stay intact after the laminate is subjected to the detonation impact. The enlarged view indicates a certain width of the laminate within the distance of the weakened groove has completely break into small debris. The surface near the LSC shows some single-layer fragments falling off but not completely. This phenomenon comes out of the joint effect of initial cutting of LSC jet and the action of tensile stress wave. The tensile stress wave is the reflection of the compressive wave generated by the jet impact on the free surface. In addition, it can be found that delamination occurred along the laminate thickness direction and the delamination phenomenon near the weakened groove is also more significant as shown in Figure 6(c). It is also found that the cutting width of the B region is larger than that of the A region. In Figure 6(d), for the cutting fracture, A region (away from the weakened groove) is relatively flat and B region (near the weakened groove) is rough with more prominent serrated burrs.

3.2. Microscopic Analysis of the Cutting Fracture. In order to study the microscopic fracture of CFRP composites after cutting, SEM (Hitachi S-4800) is used to analyze the failure cross-section of the laminates after cutting by LSC jet. In order to facilitate the observation, the size of the observation area of specimens from the cutting plate is about 20 cm × 15 cm. The microscopic images corresponding to triangles and rectangles are as marked in Figure 7(a).

The SEM images of CFRP specimens tested under LSC jet are shown in Figures 7(b)–7(f). These micrographs clearly illustrate the dominant failure mode of the laminates due to three factors: shear brittle fracture of the fiber, delamination of the composite laminates, and tensile failure of the laminates. The laminate behaves more like brittle materials because of the presence of inertia and wave propagation effects [18]. The ends of the broken fiber are flat, indicating a brittle failure which is caused by the shear loading, as shown in Figures 7(b) and 7(c). Similar phenomena can also be observed in the impact tests of the other composite laminates that are not used as a separation device [19]. There are also signs of matrix adhering to the fibers, which indicates an ideal bond on the fiber-matrix interface. The phenomenon of fiber pullout implies that the impact of jet and shock waves can cause the laminate materials at different ply angles to break under tensile loading, as shown in Figure 7(d). There are many pits formed when tensile load is applied as shown in Figure 7(e) [20]. In addition, the phenomenon of delamination along the thickness direction casued by weak interface

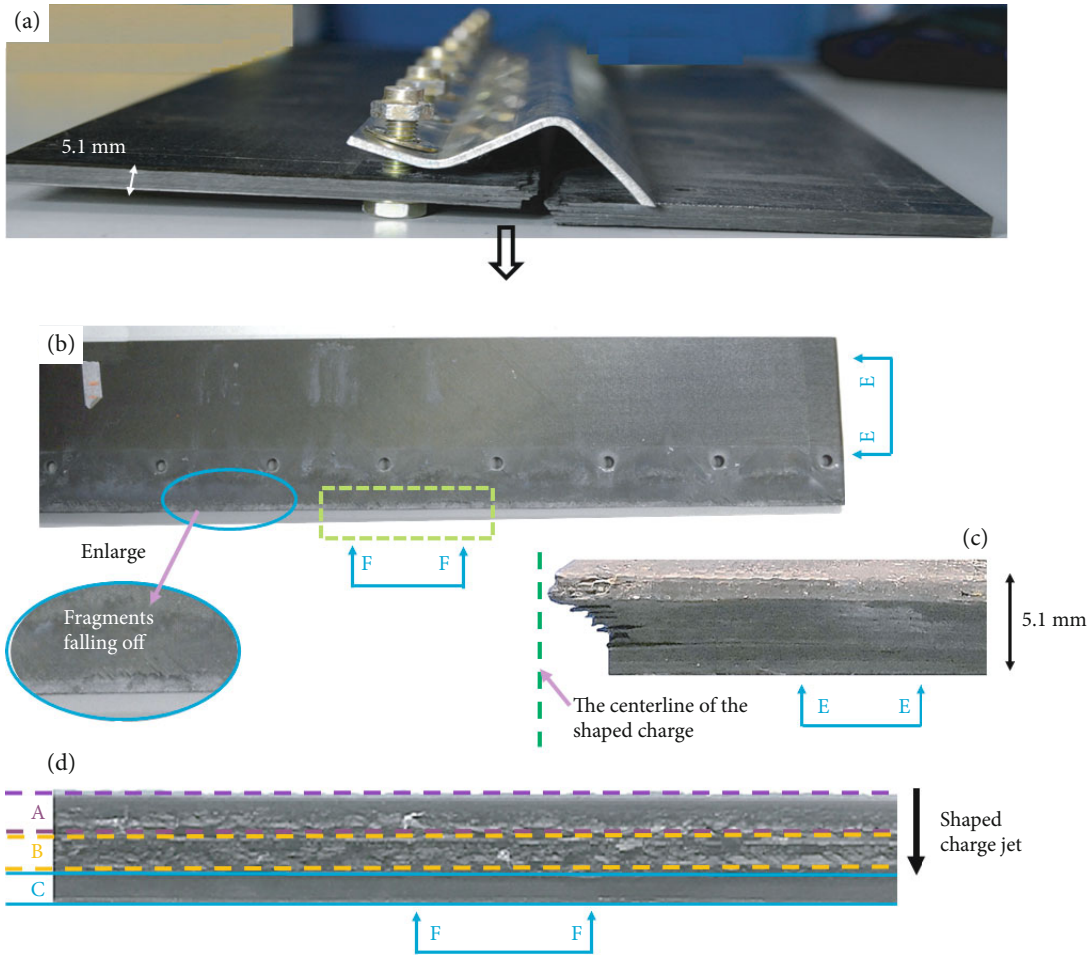

Figure 6: Macroscopic analysis. (a) Composites separation device. (b) Front view. (c) Side view. (d) Cutting fracture.

can be observed. It should be pointed out that single fiber is almost wrapped up and only fiber bundles are visible in Figure 7(f). For this phenomenon, two possible reasons are provided in this paper. Firstly, the resin is melted by high temperature and it is possible to wrap the fiber under the action of the jet. Secondly, as the cutting depth increases, the metal jet will accumulate at the bottom of the laminate and will also cover the fiber.

3.3. Evolution of the Cutting Fracture by Simulation Method

3.3.1. The Cutting Process of the Laminate. In this paper, the cutting width represents the distance between failure elements and the centerline of LSC as shown in Figure 8(a). The laminate is cut into two plates and the average cutting width of the left plate and the right plate is obtained based on the definition of cutting, and the results are provided in Figure 8. The average cutting width of the sublayers has an increasing trend with the growth of cutting depth. The damage of the laminate mainly shows within 6 mm from the weakened groove. Figure 9 shows the cutting process of the laminate. It is clear that the cutting width is smaller by the side of the shaped charge and the width is larger by the side of the weakened groove, indicating the both side cutting fractures of the laminate have shear failure and tensile failure, respectively. The reason is in the initial stage of the cutting process; the materials neighboring to the high speed jet has limited time to respond and result in a local transverse shear failure under high-speed and high-pressure conditions. The layers near the back of the composite mostly show tensile failure mode. Similar phenomena were observed in the impact tests of some other CFRP composites [21] and high-velocity impact simulation of the laminates [22].

In term of the delamination, the distance change between layers, from layer 1 to layer 21, is obtained according to the enlarged area as shown in Figure 9. The distance between adjacent layers is 0.15 mm before cutting. Figure 10 shows the distance change between layers after cutting. It shall be noted that there are some delamination distances less than 0.15 mm, which may caused by the laminate warping under the action of detonation. Different the cutting stage will show different failure mode. The 20 layers are divided into a front 10 layers and a back 10 layers, and the average delamination distance between the front 10 layers is 0.20 mm and that between the back 10 layers is 0.47. It is clear that the delamination of the back 10 layers is larger than that of the front 10 layers, and the delamination phenomenon of the laminate near the weakened groove is much larger than that of far

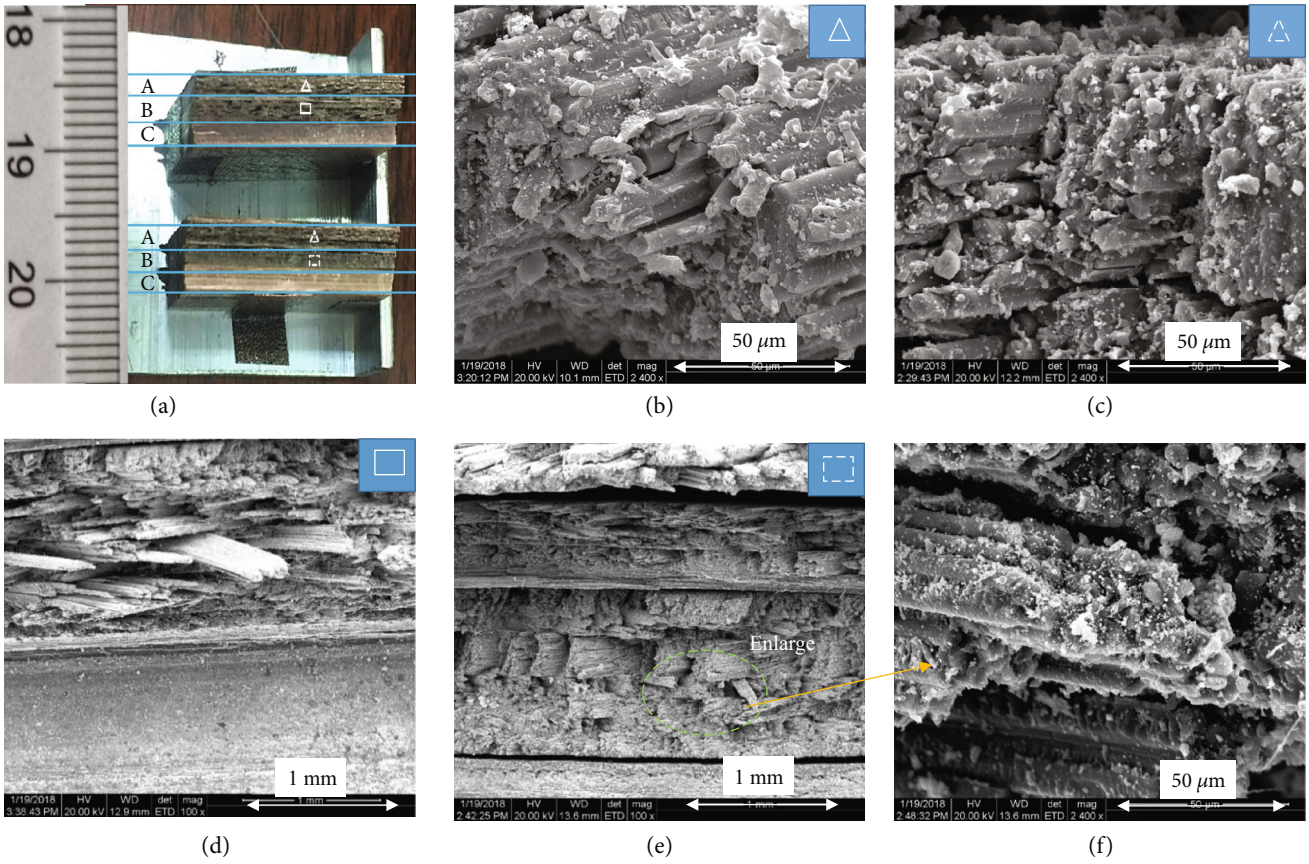

Figure 7: Cutting specimens and SEM micrographs. (a) Cutting specimens for SEM analysis. (b, c) Shear brittle fracture of fibers. (d–f) Tensile failure. Indicators A, B, and C represent the region away from weakened groove, the region near weakened groove, and the weakened groove, respectively.

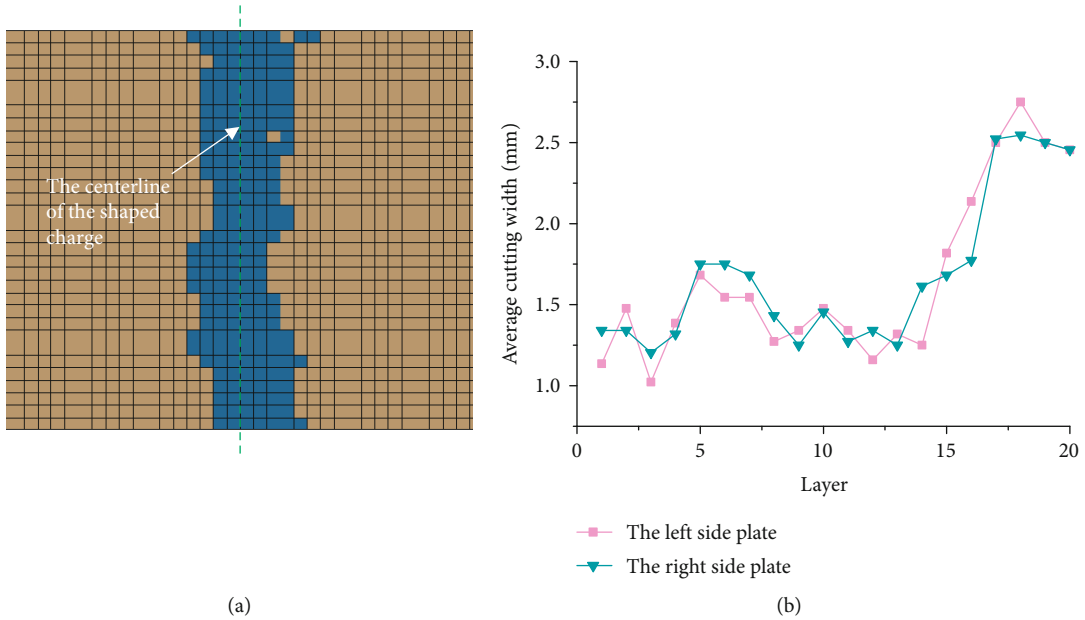

Figure 8: Cutting width. (a) Statistical view of cutting width (blue elements represent failure elements). (b) Average cutting width of the sublayers.

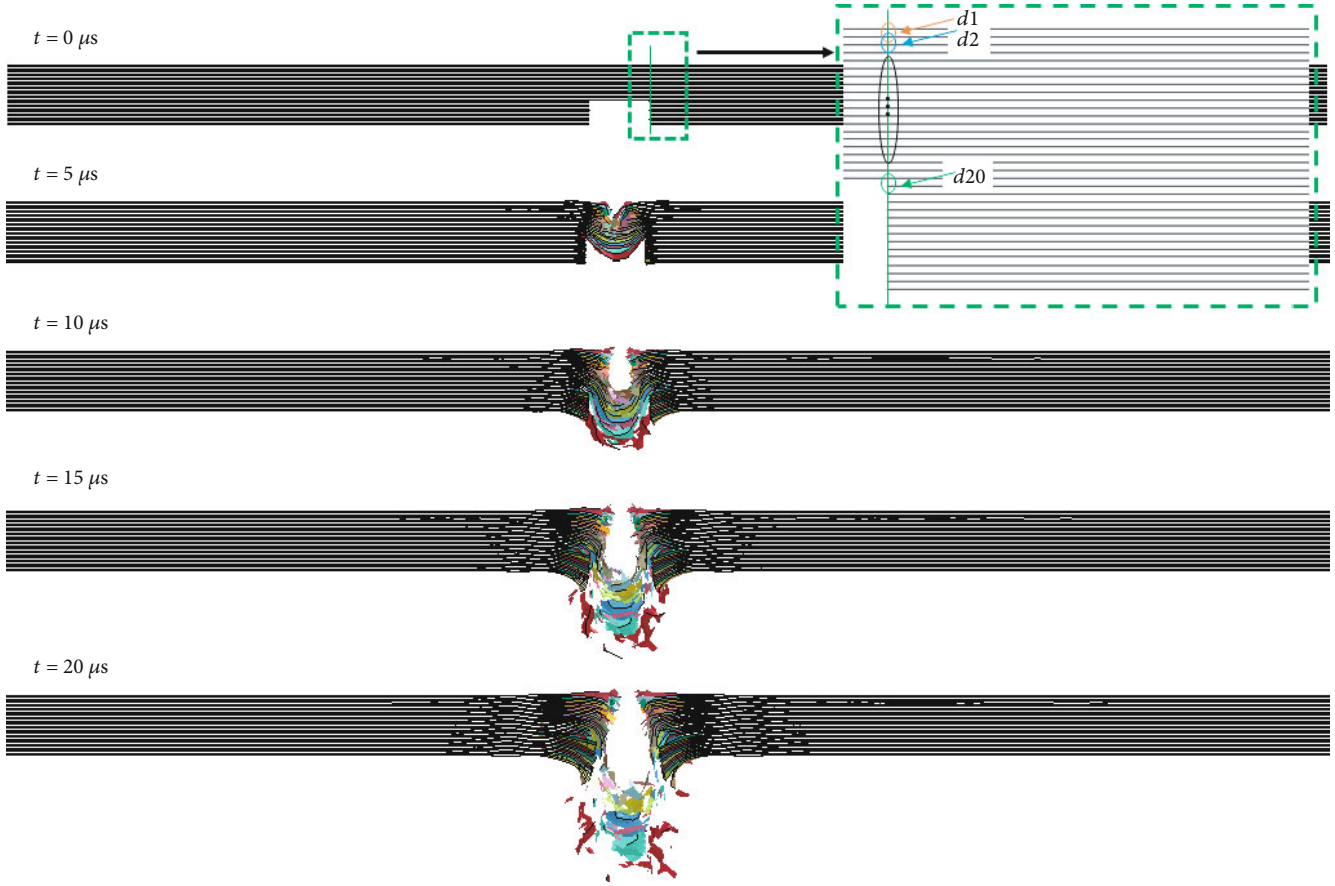

Figure 9: Cutting process of the laminate.

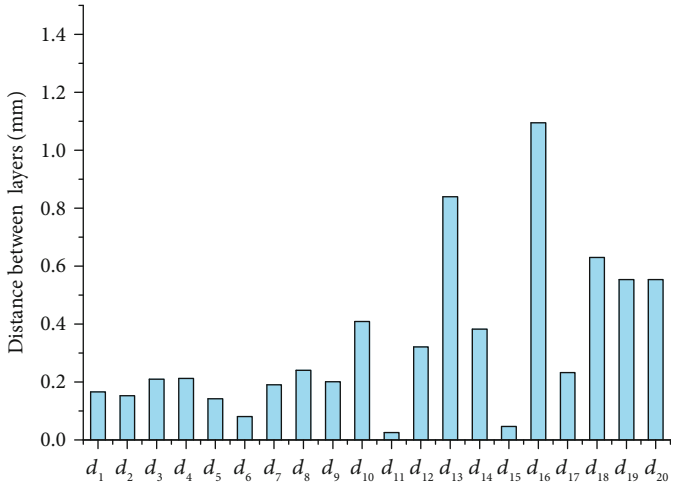

Figure 10: Delamination between layers.

away from the weakened groove, which is consistent with experiment results.

3.3.2. Change of Jet Velocity during the Cutting Process. The jet velocity is an important factor for the failure analysis of CFRPs, and several observation nodes on the outermost elements are studied during the cutting process as shown in Figure 11(a). Figure 11(b) shows the change of z-direction velocity at observation nodes. Firstly, when the jet arrives at node A, the velocity is up to 1985.07 m/s. The jet velocity at node B is almost 2176.54 m/s. At about $t = 3.0\ \mu$s, the velocity at node A and node B shows positive z-direction value which is caused by the reflections of the detonation created after contacting with the laminate surface. Nodes C, D, E, and F

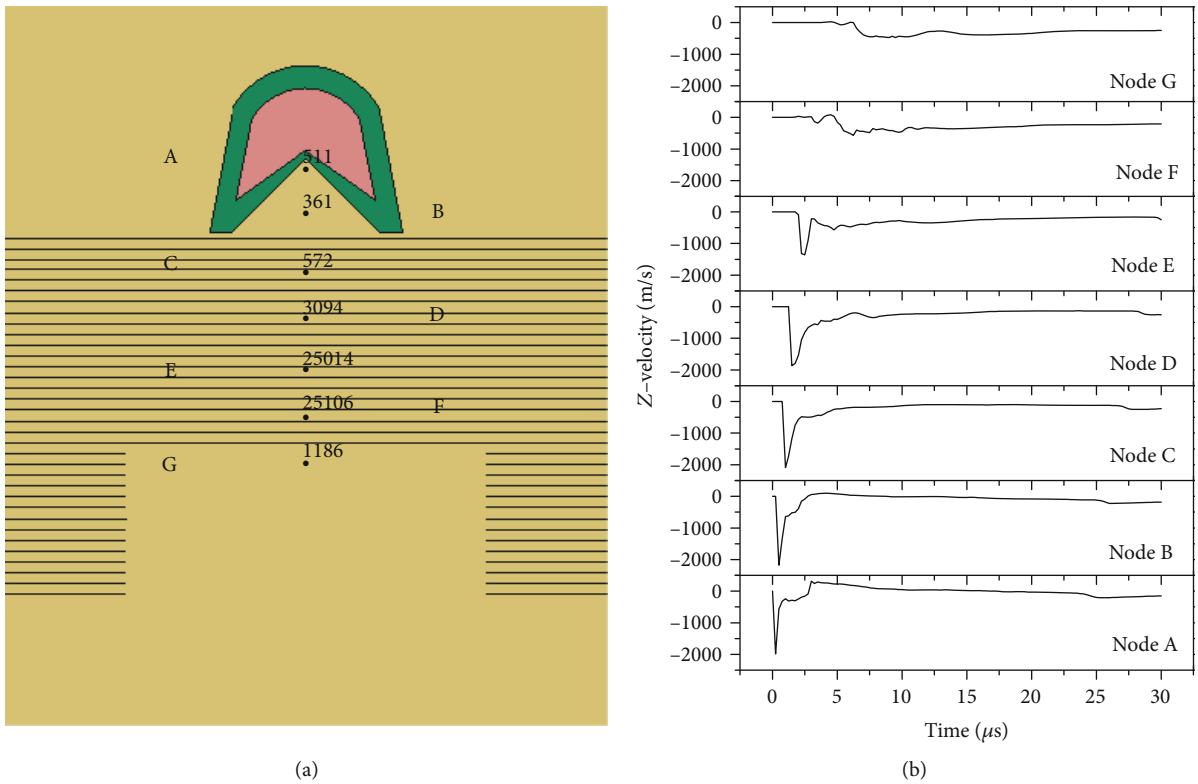

(a) (b)

Figure 11: Jet velocity. (a) Location of the velocity observation nodes. (b) Velocity curves of observation nodes.

are located in the laminate region. As the hindering effect of the laminate, the velocity of these nodes is decreasing. The maximum velocity of nodes C, D, E, and F is 2088, 1863.09, 1356.16, and 568.03 m/s, respectively. It is found that the velocity curve of node E obviously decreases and then continues to increase at about $t = 3.25\,\mu$s, which is because of the inconsistent or broken phenomenon of the jet during continuous movement. For node F, the hindering effect of the laminate is becoming more and more obvious and the maximum velocity is 74% lower than the velocity at node B. Node G is located on the outside of the laminate. The jet still has a certain velocity after it penetrates the 5.1 mm laminate and finally reaches 471.77 m/s. Since the jet velocity has been greatly reduced after the jet has penetrated the laminate, the maximum velocity at node G does not happen at the time of the original arrival of the jet but it is at the arrival of the subsequent jet.

3.3.3. In-Plane Failure in the Cutting Process of the Laminate. The cutting process of the sublayers of the laminate is analyzed in Figure 12. Layer 4 is away from the weakened groove and layer 15 is near the weakened groove. The layer directions of layer 4 and layer 15 are both 45°. It is obvious that layer 4 is cut directly by the jet. As the cutting proceeding, the jet morphology collapses and the stress wave arrives the subsequent laminate before the jet; the stress wave forms a tensile effect on the free surface reflection of the laminate [23]. Therefore, layer 15 is cut by the action of both jet and stress wave.

Figure 13 shows the in-plane failure of the sublayers over time. The above simulation has pointed out that the longitudinal and the transverse represent fiber and matrix, respectively. The right fringe levels show the damage degree of elements. The blue paint represents no damage while the red paint represents the greatest damage. For layer 4, the initial time of damage of the fiber and the matrix near the shaped charge shows less difference at $t = 1.75\,\mu$s. As for the cutting progress, there is no significant difference between the damage area in fiber and matrix. Under the initial high-speed jet, the damage of the fiber and the matrix has limited time to respond to the stress wave, and the materials mostly fail due to the direct shear loading. Layer 4 shows a uniform and flat cross-section along the shaped charge direction after cutting, which is a typical shear failure. In terms of layer 15, the damaged area of the matrix is significantly larger than that of the fiber at $t = 3.5\,\mu$s, and the rate of damage in the matrix increases in the later cutting stage. In this case, the fibers are directly exposed to the air after the matrix damage, and the fracture of layer 15 is relatively rough when the jet velocity reduces and the jet form collapses. Therefore, the shear failure is the dominant failure mode at the areas away from weakened grooves, while the tensile failure is the dominant failure mode at the areas near the weakened groove.

3.4. Failure Analysis of CFRPs Subjected to LSC. Through the abovementioned tests and FE simulation, the failure analysis of CFRPs subjected to shaped charge jet is summarized here.

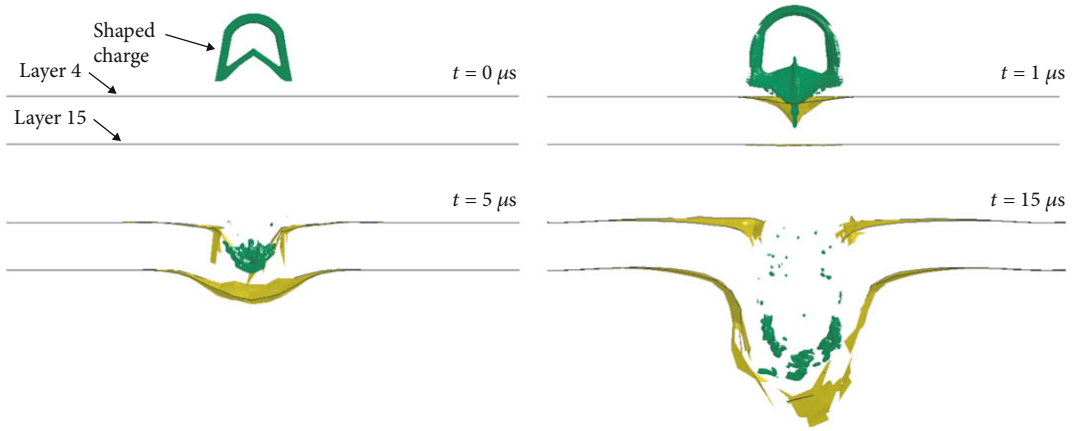

Figure 12: Cutting process of the sublayer.

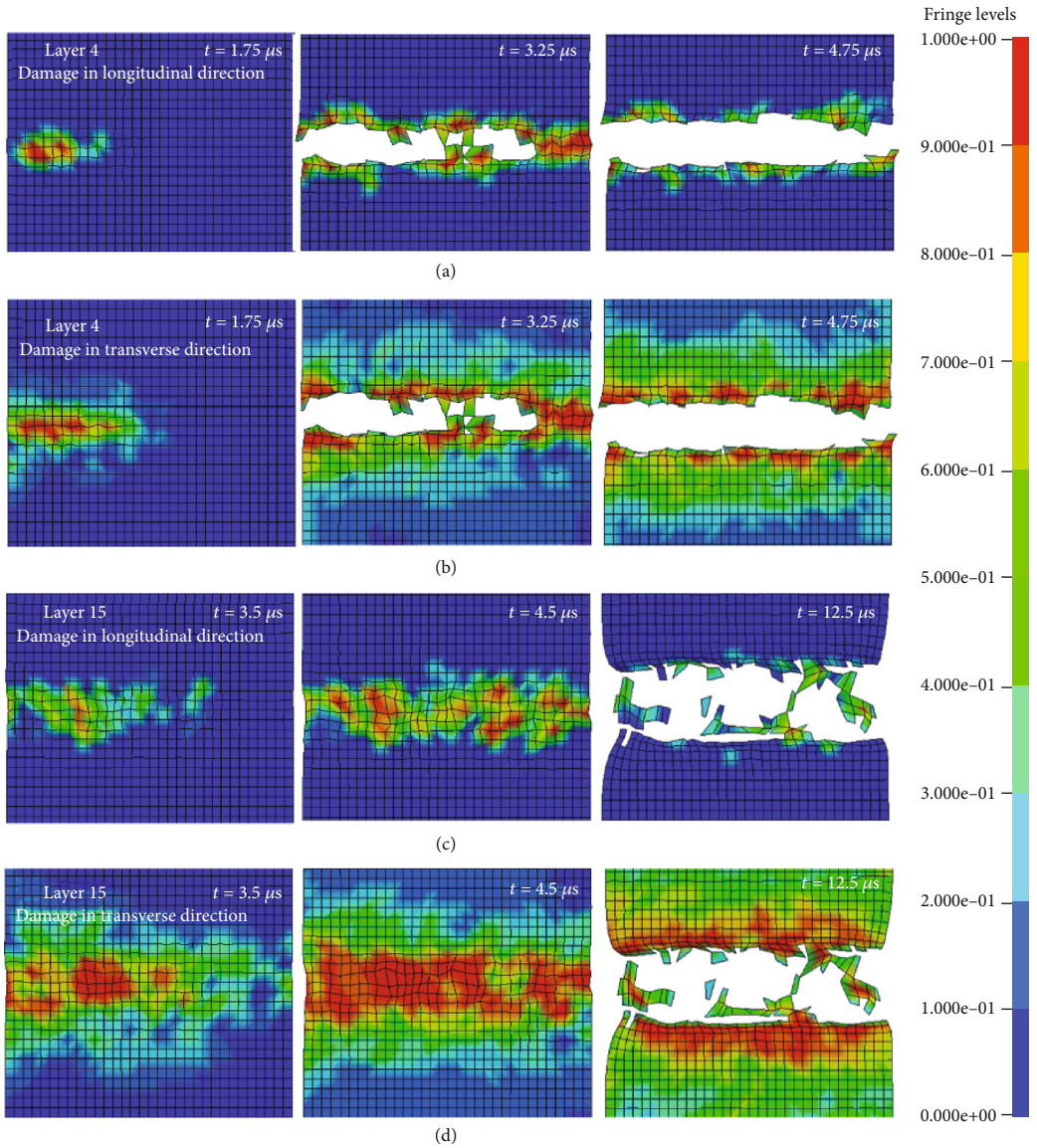

Figure 13: Comparison of in-plane failure in the sublayers (a, c). Damage in longitudinal direction for layer 4 and layer 15 (b, d). Damage in transverse direction for layer 4 and layer 15.

Firstly, there is a detachment of laminate surface caused by the erosion of the shaped charge jet and the tension effect due to the reflection of compressive stress wave from the macroscopic analysis. Secondly, from the macroscopic and microscopic fracture observation, the laminate fracture near the shaped charge is relatively uniform, and the end of fibers is flat due to the shear failure mode. For the uniform fracture, as the LSC forms steadily in this stage, the initial jet velocity is high and the shape of jet is thinner in FE modeling. There is no significant difference in the damage time and damage area of the fiber and matrix for the in-plane failure of the laminate. Therefore, the laminate is directly separated by the high-speed jet, and its uniform fracture and flat breakage along the shaped charge direction indicate a shear failure mode. Thirdly, as for the cutting progress, the cutting fracture near the weakened groove is rough with more prominent serrated burrs and lots of fiber pullout and pits, which implies a tensile failure mode in the microscopic characterization. In terms of the rough fracture, the hindering effect increases, the jet velocity decreases, and the jet morphology collapes. The damage of the matrix precedes the fiber, and the area of damage is significantly larger than that of the fibers. The exposure of fibers leads to a tensile failure mode of the laminates, which is relatively rough compared with the stage with high-speed jet. From the perspective of stress wave effect, the stress wave arrives at the laminate before the jet, which causes a tensile failure mode under the action of both jet cutting and reflective stress wave. It is also found that due to the different failure modes of the laminates, the cutting width of several layers of the laminate near the weakened groove becomes larger than the region away from the weakened groove. Moreover, there has always been delamination phenomenon under the coupling action of the jet and stress wave propagation during the cutting process. In particular, the delamination of the laminate in the subsequent cutting is larger than that of the precutting stage.

4. Conclusions and Remarks

In this paper, the cutting test of CFRP-based pyrotechnic separation device is carried out and finite element anlaysis (FEA) is employed to conduct failure analysis of CFRPs under linear shaped charge (LSC). Firstly, in terms of fracture morphology and main failure mode of the laminate, the simulation results of CFRP composites subjected to LSC jet are consistent with experimental results, which proves the reliability of FEA in the modeling of pyrotechnic separation devices. Secondly, the cutting fracture of CFRPs can be divided into two sections. In the upper section near the shaped charge, the fracture is relatively uniform with flat end of the fiber, indicating a shear failure mode. For the uniform fracture, the jet velocity is large and the jet shape is compact in numerical simulation. There is no significant difference in the damage time and damage area of the fiber and matrix for the in-plane failure of the laminate, and the laminate was directly seperated by the high-speed jet. For the lower section near the weakened groove, fiber pullout and pits frequently occur in the fracture cross-section and the cutting fracture is relatively rough due to a tensile failure mode. When the jet velocity decreases and the morphology collapses, matrix damage would precede into the fiber. At the same time, the fiber exposure leads to a tensile failure mode, explaining the rough cross-section after the jet cutting. In addition, delamination happens during the cutting process because the interfacial strength between the layers is not strong enough to resist the jet impact and the complex stress wave. This delamination phenomenon of the laminate is more severe in the stage with lower jet speed. To sum up, detailed failure analyses were conducted in this paper to provide an insightful understanding about the failure of CFRPs in pyrotechnic separation devices. On basis of the jet velocity and morphology, the cutting process can be divided into different stages and the failure mode of CFRPs significantly vary with the cutting stage, which is critical to evaluate the quality of separation using these pyrotechnic separation devices. Advanced pyrotechnic separation devices shall better control the jet shape and speed, which can increase the proportion of shear fracture and decrease the chance of tensile fracture and delamination. The failure mode study proposed in this paper can explain the performance of current pyrotechnic separation devices and be used as a evaluation protocol in the future optimization of CFRP-based pyrotechnic separation devices.

Data Availability

The data used to support the findings of this study are included within the article.

Conflicts of Interest

The authors declare that there are no competing interests regarding the publication of this paper.

Acknowledgments

This study is supported by the Chinese National Natural Science Foundation (Nos. 11602030 and U1837204) and the Aeronautical Science Foundation of China (No. 2017ZE63011). The authors thank the Beijing Institute of Astronautical Systems Engineering for the support during the experimental characterizations.

References

[1] J. F. Molinari, "Finite element simulation of shaped charges," *Finite Elements in Analysis and Design*, vol. 38, no. 10, pp. 921–936, 2002.

[2] Y. Li, Z. Xiang, G. Y. Bing, and H.-Q. Liu, "An experimental study on use of Li near cumulative charge for cutting of steel plate," *Engineering Blasting*, vol. 9, no. 2, pp. 19–21, 2003.

[3] T. Xian-Shu, W. Shu-Min, and Z. Guo-Feng, "Experimental and numerical simulating study on the capacity of the linear shaped charge cutting the shape steel," *Journal of Jinggangshan University*, vol. 34, no. 6, pp. 66–71, 2013.

[4] D. Z. Lyu, W. R. Hong, M. C. Yuan, and H. J. Xuan, "Spallation affected fracture pattern of a titanium alloy plate subjected to linear shaped charge jet penetration," *Combustion, Explosion, and Shock Waves*, vol. 53, no. 3, pp. 362–369, 2017.

[5] S. O. N. G. Bao-yong, H. L. Lu, Z. G. Yang et al., "Studies on fracture mechanism of explosive separation device subjected to impact loads," *Acta Armamentarii*, vol. 30, no. S2, pp. 102–106, 2009.

[6] Z. Zhang, L. Wang, V. V. Silberschmidt, and S. Wang, "SPH-FEM simulation of shaped-charge jet penetration into double hull: a comparison study for steel and SPS," *Composite Structures*, vol. 155, pp. 135–144, 2016.

[7] X. Jia, Z. X. Huang, M. Guo, X. D. Zu, and L. Ji, "Study on impact response of laminated woven fabric rubber composite armour against shaped charge jet," *Plastics, Rubber and Composites*, vol. 44, no. 9, pp. 351–361, 2015.

[8] R. A. W. Mines, A. M. Roach, and N. Jones, "High velocity perforation behaviour of polymer composite laminates," *International Journal of Impact Engineering*, vol. 22, no. 6, pp. 561–588, 1999.

[9] R. Kapoor, L. Pangeni, A. K. Bandaru, S. Ahmad, and N. Bhatnagar, "High strain rate compression response of woven Kevlar reinforced polypropylene composites," *Composites Part B Engineering*, vol. 89, pp. 374–382, 2016.

[10] S. W. R. Lee and C. T. Sun, "On the apparent bending isotropy in clamped elliptic composite laminates," *Journal of Composite Materials*, vol. 29, no. 12, pp. 1601–1620, 1995.

[11] W. L. Cheng, S. Langlie, and S. Itoh, "High velocity impact of thick composites," *International Journal of Impact Engineering*, vol. 29, no. 1–10, pp. 167–184, 2003.

[12] Z. Zhang, L. Wang, and V. V. Silberschmidt, "Damage response of steel plate to underwater explosion: effect of shaped charge liner," *International Journal of Impact Engineering*, vol. 103, pp. 38–49, 2017.

[13] D. Q. Cao, S. R. Yun, G. Y. Ding, and Q. K. Jin, "3-D numerical simulation of jet penetrate target using ALE method," *Journal of Beijing Institute of Technology*, vol. 2, 2000.

[14] Livermore Software Technology Corporation (LSTC), *LSDYNA: Keyword User's Manual – Volume I: Material Models*, CAL, 2012.

[15] Livermore Software Technology Corporation (LSTC), *LSDYNA: Keyword User's Manual – Volume II: Material Models*, CAL, 2012.

[16] M. zhiguo, *Research on Impact Fracture Behavior of Carbon Fiber Laminates under Explosive of Linear Shaped Charge*, Graduate School of National University of Defense Technology, Changsha, 2016.

[17] A. Matzenmiller, J. Lubliner, and R. L. Taylor, "A constitutive model for anisotropic damage in fiber-composites," *Mechanics of Materials*, vol. 20, no. 2, pp. 125–152, 1995.

[18] K. Naresh, K. Shankar, B. S. Rao, and R. Velmurugan, "Effect of high strain rate on glass/carbon/hybrid fiber reinforced epoxy laminated composites," *Composites Part B Engineering*, vol. 100, pp. 125–135, 2016.

[19] O. I. Okoli and G. F. Smith, "Failure modes of fibre reinforced composites: the effects of strain rate and fibre content," *Journal of Materials Science*, vol. 33, no. 22, pp. 5415–5422, 1998.

[20] U. Tamilarasan, L. Karunamoorthy, and K. Palanikumar, "Mechanical properties evaluation of the carbon fibre reinforced aluminium sandwich composites," *Materials Research*, vol. 18, no. 5, pp. 1029–1037, 2015.

[21] G. D. Roberts, D. M. Revilock, W. K. Binienda, W. Z. Nie, S. B. Mackenzie, and K. B. Todd, "Impact testing and analysis of composites for aircraft engine fan cases," *Journal of Aerospace Engineering*, vol. 15, no. 3, pp. 104–110, 2002.

[22] L. Zhu, A. Chattopadhyay, and R. K. Goldberg, "Failure model for rate-dependent polymer matrix composite laminates under high-velocity impact," *Journal of Aerospace Engineering*, vol. 21, no. 3, pp. 132–139, 2008.

[23] X. Gu, X. Xu, and J. Huang, "High velocity impact damage of thin composite laminates," *Journal of Nanjing University of Aeronautics & Astronautics*, vol. 40, no. 3, pp. 370–375, 2008.